LabAnimal

ARTICLES

https://doi.org/10.1038/s41684-023-01238-6

Check for updates

OPEN

Development of two mouse strains conditionally expressing bright luciferases with distinct emission spectra as new tools for in vivo imaging

Toshiaki Nakashiba[1]✉, Katsunori Ogoh[2], Satoshi Iwano[3,7], Takashi Sugiyama[2,8], Saori Mizuno-Iijima[1], Kenichi Nakashima[4], Seiya Mizuno[5], Fumihiro Sugiyama[5], Atsushi Yoshiki[1], Atsushi Miyawaki[3] and Kuniya Abe[6]

In vivo bioluminescence imaging (BLI) has been an invaluable noninvasive method to visualize molecular and cellular behaviors in laboratory animals. Bioluminescent reporter mice harboring luciferases for general use have been limited to a classical luciferase, Luc2, from *Photinus pyralis*, and have been extremely powerful for various in vivo studies. However, applicability of reporter mice for in vivo BLI could be further accelerated by increasing light intensity through the use of other luciferases and/or by improving the biodistribution of their substrates in the animal body. Here we created two Cre-dependent reporter mice incorporating luciferases oFluc derived from *Pyrocoeli matsumurai* and Akaluc, both of which had been reported previously to be brighter than Luc2 when using appropriate substrates; we then tested their bioluminescence in neural tissues and other organs in living mice. When expressed throughout the body, both luciferases emitted an intense yellow (oFluc) or far-red (Akaluc) light easily visible to the naked eye. oFluc and Akaluc were similarly bright in the pancreas for in vivo BLI; however, Akaluc was superior to oFluc for brain imaging, because its substrate, AkaLumine-HCl, was distributed to the brain more efficiently than the oFluc substrate, D-luciferin. We also demonstrated that the lights produced by oFluc and Akaluc were sufficiently spectrally distinct from each other for dual-color imaging in a single living mouse. Taken together, these novel bioluminescent reporter mice are an ideal source of cells with bright bioluminescence and may facilitate in vivo BLI of various tissues/organs for preclinical and biomedical research in combination with a wide variety of Cre-driver mice.

Bioimaging constitutes an essential part of research in the life sciences, as it provides a wide array of tools for analyses of molecular and cellular behaviors in various biological systems. Since the advent of fluorescent protein (FP) technology, live imaging has revolutionized the fields of cell biology because, in theory, any gene product or type of cell can be marked and traced[1]. However, it has been challenging to apply FP technology to live imaging at the organismal level. The excitation light required for FP technology in biological tissues is severely attenuated because of light scattering and absorption, rendering in vivo live imaging using FP impractical[2,3]. Furthermore, the excitation light causes 'autofluorescence' from biological materials, such as NADPH and flavoproteins, which exacerbates the signal-to-noise ratio of FP signals[4,5].

By contrast, bioluminescence imaging (BLI) using bioluminescent luciferase/luciferin systems has a wider dynamic range than fluorescent imaging because of the lack of requirement for excitation light[6,7]. BLI is considered to be a more suitable modality for noninvasive deep-tissue imaging. Among the bioluminescent luciferase/luciferin systems, the luciferase from the firefly *Photinus pyralis*, and particularly its derivative Luc2, has been the most widely used reporter; it produces an orange light by oxidizing D-luciferin (peak emission at 609 nm)[8]. Although reporter mice possessing Luc2 have been widely used for in vivo BLI[9–17], some issues remain, for example, relatively weak light intensity produced from the luciferase and the limited biodistribution of D-luciferin, which distributes poorly within the brain because of the blood–brain barrier (BBB)[18,19].

For better in vivo BLI, attempts have been made to increase the light intensity and improve the biodistribution of substrates. As synthetic compounds of D-luciferin derivative, CycLuc1, and AkaLumine hydrochloride (AkaLumine-HCl) exhibit enhanced biodistribution in most tissues including brain and produce red-shifted light, which could result in a better penetration of animal tissues and bodies (the peak emission of Luc2 is at 604 nm for CycLuc1 and at 677 nm for AkaLumine-HCl)[20,21]. Meanwhile, novel luciferase derivatives with a brighter light intensity and/or red-shifted wavelength have been searched[22–24]. Although a red-shifted wavelength was achieved by site-directed mutagenesis of Luc2 using D-luciferin as a substrate, the total photon yield in most of these mutants did not exceed that produced by the original Luc2 (ref. [23]). This poor yield was also the case when combining Luc2 and the synthetic luciferins mentioned above[25]. More recently, Iwano et al.[26] reported the development of the AkaBLI system, in which an innovative derivative of Luc2, Akaluc, was used in conjunction with AkaLumine-HCl. Remarkably, Akaluc produced a luminescent signal that was ten times brighter than that produced by Luc2 when measured in vitro. Even more remarkably, the difference exceeded 100-fold for in vivo BLI, probably because

[1]Experimental Animal Division, RIKEN BioResource Research Center, Tsukuba, Japan. [2]Corporate Research and Development Center, Olympus Corporation, Hachioji, Japan. [3]Laboratory for Cell Function and Dynamics, RIKEN Center for Brain Science, Wako, Japan. [4]Gene Engineering Division, RIKEN BioResource Research Center, Tsukuba, Japan. [5]Laboratory Animal Resource Center in Transborder Medical Research Center, Institute of Medicine, University of Tsukuba, Tsukuba, Japan. [6]Technology and Development Team for Mammalian Genome Dynamics, RIKEN BioResource Research Center, Tsukuba, Japan. [7]Present address: Institute for Tenure Track Promotion, University of Miyazaki, Miyazaki, Japan. [8]Present address: R&D Division, Evident Corporation, Hachioji, Japan. ✉e-mail: toshiaki.nakashiba@riken.jp

of the emission peak of AkaBLI at 650 nm, which is within the range of the 'optical window of biological tissues'[4]. In fact, single cells trapped in the mouse lung could be detected using the AkaBLI system[26]. This newly developed BLI system should open new avenues of research involving deep-tissue imaging.

Newly developed BLI systems have been mostly evaluated in in vivo settings by injecting cells or viral vectors carrying luciferase genes into small animals[20,21,23,25–28]. However, these methods are limited to cells that are amenable to viral transduction and to several spatial locations in the body that are accessible using procedures such as the pulmonary trapping of intravenously injected cells or subcutaneous cellular transplants. Furthermore, surgical procedures for viral injection or cellular transplants may have various consequences in different animals when considering the number of cells and their spatial location, thus complicating the evaluation of BLI systems. Therefore, the next logical step in the development of the BLI system is the generation of genetically modified mouse strains in which the BLI system can be systematically operated by genetic means.

Another item to add to the BLI toolbox would be bright luciferases with an emission peak distinct from that of Akaluc. Multicolor imaging is critical and advantageous for bioimaging to detect and analyze the behaviors or interactions of more than two elements in biological systems (as exemplified by multicolor imaging using multiple FPs with distinct emission peaks). However, for in vivo BLI, luciferases that are as bright as Akaluc but exhibit different emission peaks have not yet been reported. Ogoh et al.[29] isolated and characterized a luciferase derived from the firefly *Pyrocoeli matsumurai*, which inhabits Okinawa Island of Japan. This luciferase (hereinafter referred to as oFluc) produces yellow light (peak emission at 567 nm) when D-luciferin is used as a substrate, and its luminescence intensity is ten times brighter than that produced by Luc2 when measured in cultured cells[29]. While Akaluc was found not to catalyze D-luciferin for light production[26], the substrate specificity of oFluc has not yet been clarified. Based on the assumption that oFluc does not produce light with AkaLumine-HCl, we envisaged that oFluc might be an ideal partner for Akaluc for dual-color BLI using both substrates.

In this Article, we generated two mouse strains, in which Cre-dependent reporter constructs carrying Akaluc and oFluc were inserted into the *ROSA26* locus, which is a safe harbor site in the mouse genome for stable expression[30]. By crossing with a general-deleter Cre strain, we created 'glowing mice' that exhibited whole-body bioluminescence, thus representing an ideal source of various bioluminescence-emitting cells to suit a wide variety of transplantation studies. These mouse strains can certainly be directed to express the luciferase reporters in specific cell populations using the Cre/loxP recombination system, thereby allowing the noninvasive imaging of specific cell populations in the whole body. Furthermore, this system should be helpful in locating cell domains undergoing Cre-mediated recombination during development and adulthood. Although such Cre-mediated expression of Luc2 in the mouse has been reported[31–34], the use of much brighter BLI systems, such as Akaluc and oFluc, with distinct emission peaks will undoubtedly expand the utility of the reporter lines for both basic and preclinical research. Here we demonstrated the feasibility of in vivo dual-color BLI in a single living mouse that harbored both the Akaluc and oFluc reporters.

Results

Generation of oFluc and Akaluc reporter mice. We aimed to introduce reporter constructs (Fig. 1a) carrying oFluc or Akaluc into the *ROSA26* locus, a safe harbor for stable expression in the mouse genome. The expression of the luciferases was driven by the strong and ubiquitous *CAG* promoter[35]. A floxed transcription stop cassette—the neomycin resistance gene (*Neo*) followed by SV40 poly A—was placed between the *CAG* promoter and the reporter. The stability of the reporter mRNA was further enhanced by the woodchuck hepatitis virus post-transcriptional regulatory element (WPRE)[36]. The Akaluc-encoding complementary DNA was fused at its N terminus with the coding sequence for Venus, a fluorescent protein derived from green fluorescent protein (GFP)[37], to compare BLI and fluorescent imaging via equimolar expression of the two reporters (Venus/Akaluc). By contrast, oFluc was not fused to maximize its expression (Fig. 1a).

We generated two mouse strains, CAG–LSL–oFluc and CAG–LSL–Venus/Akaluc, using the clustered regularly interspaced short palindromic repeats (CRISPR)–Cas9 technique with fertilized eggs collected from C57BL/6J mice. Both strains integrated the insert DNA at the *ROSA26* locus (Fig. 1b and Supplementary Fig. 1). One copy of CAG–LSL–Venus/Akaluc was inserted into the locus, whereas two copies of CAG–LSL–oFluc were inserted with a vector backbone of the targeting vector plasmid. After crossing these animals with CAG–Cre mice[38], for germ-line recombination between loxP sites, we established two additional mouse strains, CAG–oFluc and CAG–Venus/Akaluc, both of which carried one copy of the insert DNA fragment from which the stop cassette was deleted from the *ROSA26* locus (Fig. 1c and Supplementary Fig. 1).

'Glowing mice' in two different colors. We examined the bioluminescence of CAG–oFluc and CAG–Venus/Akaluc mice in a dark room. We performed an intraperitoneal (IP) injection of 100 mM D-luciferin (5 µl per grams of body weight (g.b.w.)) into CAG–oFluc mice, and 15 mM AkaLumine-HCl (5 µl per g.b.w.) into CAG–Venus/Akaluc mice. Shortly after the IP injection into live animals, mice of both strains started emitting light, initially from their abdomen and, after 5 min, throughout their body. These signals were highly bright and even visible to the naked eye. The movements of live mice could be recorded by a consumer-grade digital color camera (Sony α7SII) at the video-frame rate (of 30 frames per second (f.p.s.)) (Fig. 1e–g and Supplementary Movie 1). Both luciferases were intensely bright in the BLI setup using an electron-multiplying charge-coupled device (EM-CCD) camera. Their signals saturated the EM-CCD sensor with an exposure of only tens of milliseconds (Fig. 1i,j). By contrast, the negative controls showed no detectable signal during the same exposure time. Signals from post-implantation embryos comprising approximately 1,000 cells[39] and carrying the reporters were successfully detected in utero at embryonic day 6.5 (E6.5) (Supplementary Fig. 2). CAG–oFluc and CAG–Venus/Akaluc mice emitted light with comparable intensity in distinct colors corresponding to their peak emissions, yellow and red, respectively (Fig. 1d–g). The injection of a synthetic luciferin, CycLuc1 (ref. [21]), into CAG–oFluc mice produced red-shifted light (Fig. 1f), which was consistent with the data obtained in vitro using recombinant luciferase proteins and substrates (Fig. 1d). Anesthetized CAG–Venus/Akaluc mice exhibited Venus fluorescence in their entire body (Fig. 1h).

Luciferase activity in tissues and their extracts. We then quantitatively assessed luciferase activity in crude tissue extracts via incubation with their appropriate substrates (Fig. 2a–c). Five groups of mice were included in this assay: CAG–oFluc, CAG–Venus/Akaluc, CAG–LSL–oFluc, CAG–LSL–Venus/Akaluc, and C57BL/6. CAG–oFluc and CAG–Venus/Akaluc mice displayed strong bioluminescent signals in all tissues examined; the increase in the signals relative to the negative control (C57BL/6) mice was on average 10^4- or 10^3-fold, respectively. By contrast, the signals in CAG–LSL–oFluc and CAG–LSL–Venus/Akaluc mice were extremely low, comparable with those of C57BL/6 mice, indicating the robust inducibility of luciferase expression in a Cre-dependent manner. Of note, these mice exhibited a slight but significant increase in signal strength over C57BL/6 mice in some tissues, such as the brain and testis (Fig. 2a–c).

The fold increase in the fluorescent intensity of Venus in CAG–Venus/Akaluc mice was not as large as that of Akaluc bioluminescence and was within the range of a 10- to 200-fold increase relative to C57BL/6 mice (Fig. 2d). This relatively small fold increase was

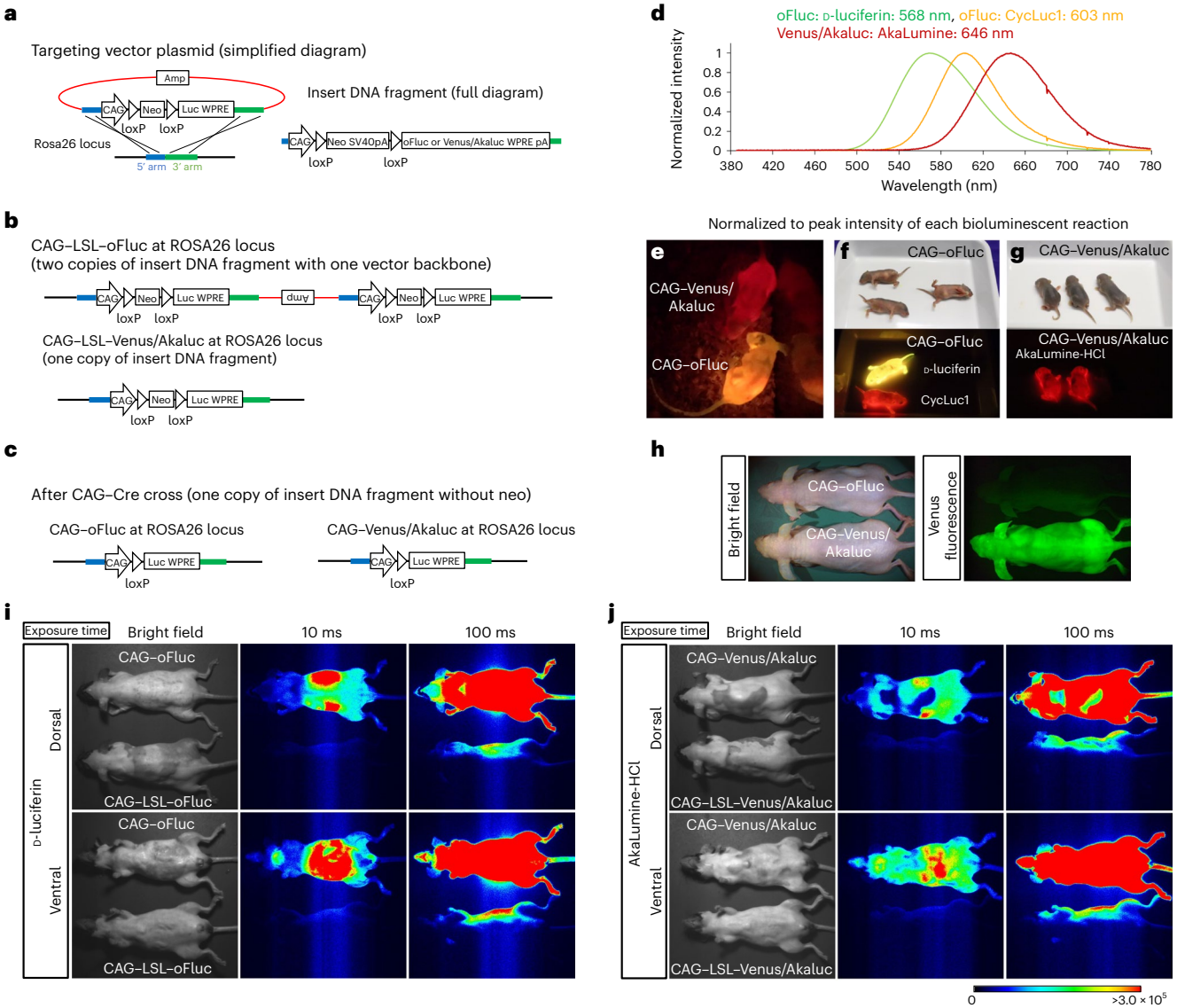

Fig. 1 | Luciferase reporter mice and in vivo BLI of 'glowing mice'. a, Simplified diagram of the targeting vector plasmid (left) for the *ROSA26* locus and a full description of the insert DNA fragment (right). The plasmid backbone, 5′ homology arm and 3′ homology arm are indicated in red, blue and green, respectively. **b**, Cre-dependent luciferase knock-in alleles at the *ROSA26* locus; two copies of the CAG–LSL–oFluc insert DNA fragment were integrated together with a plasmid backbone, whereas one copy of the CAG–LSL–Venus/Akaluc insert DNA fragment was integrated without a plasmid backbone. **c**, After the CAG–Cre cross, both CAG–oFluc and CAG–Venus/Akaluc mice had one copy of the insert DNA fragment without the *Neo* cassette. **d**, Emission spectra of luciferases with their substrates. **e**, Representative image of CAG–oFluc and CAG–Venus/Akaluc mice captured using a digital color camera at 10 min after IP injection of their substrates (100 mM D-luciferin, 5 µl per g.b.w. for CAG–oFluc; 15 mM AkaLumine-HCl, 5 µl per g.b.w. for CAG–Venus/Akaluc). Freely behaving mice were recorded at 30 f.p.s. (Supplementary Movie 1). **f**,**g**, Representative images of mice at postnatal day 4 were captured using a digital color camera after IP injection of the substrate (10 µl). The mice on the right side received no substrate injection. **h**, Venus fluorescence of CAG–Venus/Akaluc mice captured by Keyence GFP-lighting system (VB-L12). **i**,**j**, In vivo BLI images were captured using an EM-CCD camera. CAG–oFluc was compared with the negative control, CAG–LSL–oFluc (**i**), and CAG–Venus/Akaluc was compared with CAG–LSL–Venus/Akaluc (**j**), (100 mM D-luciferin, 5 µl per g.b.w. for oFluc; 15 mM AkaLumine-HCl, 5 µl per g.b.w. for Venus/Akaluc). The hair on both the dorsal and ventral sides of the mice was shaved. The signals from the bodies of CAG–LSL–oFluc and CAG–LSL–Venus/Akaluc mice reflected the light emitted from the CAG–oFluc and CAG–Venus/Akaluc mice placed next to these animals (note that the signals were found only on the near side of the bodies).

attributed to the high background signal caused by autofluorescence, whereas no such background was detected in bioluminescence, as revealed by the ex vivo imaging of tissues incubated with their appropriate substrates (Fig. 2e–g).

In vivo BLI of specific cells/organs. The experiments described above were conducted by incubating tissue extracts and dissected organs with the substrates; thus, they did not consider the biodistribution of the substrates and light penetration throughout the mouse bodies. We next directed the expression of reporter luciferases in specific tissues/organs using cell-type-specific or tissue-specific Cre-driver mice for in vivo BLI. We selected four Cre-driver strains that express Cre in neural or nonneural tissues. In vivo BLI was performed using an EM-CCD camera at 10 min after the IP injection of the substrates (100 mM D-luciferin, 5 µl per g.b.w.; 15 mM AkaLumine-HCl, 5 µl per g.b.w.). The signals were captured through a series of

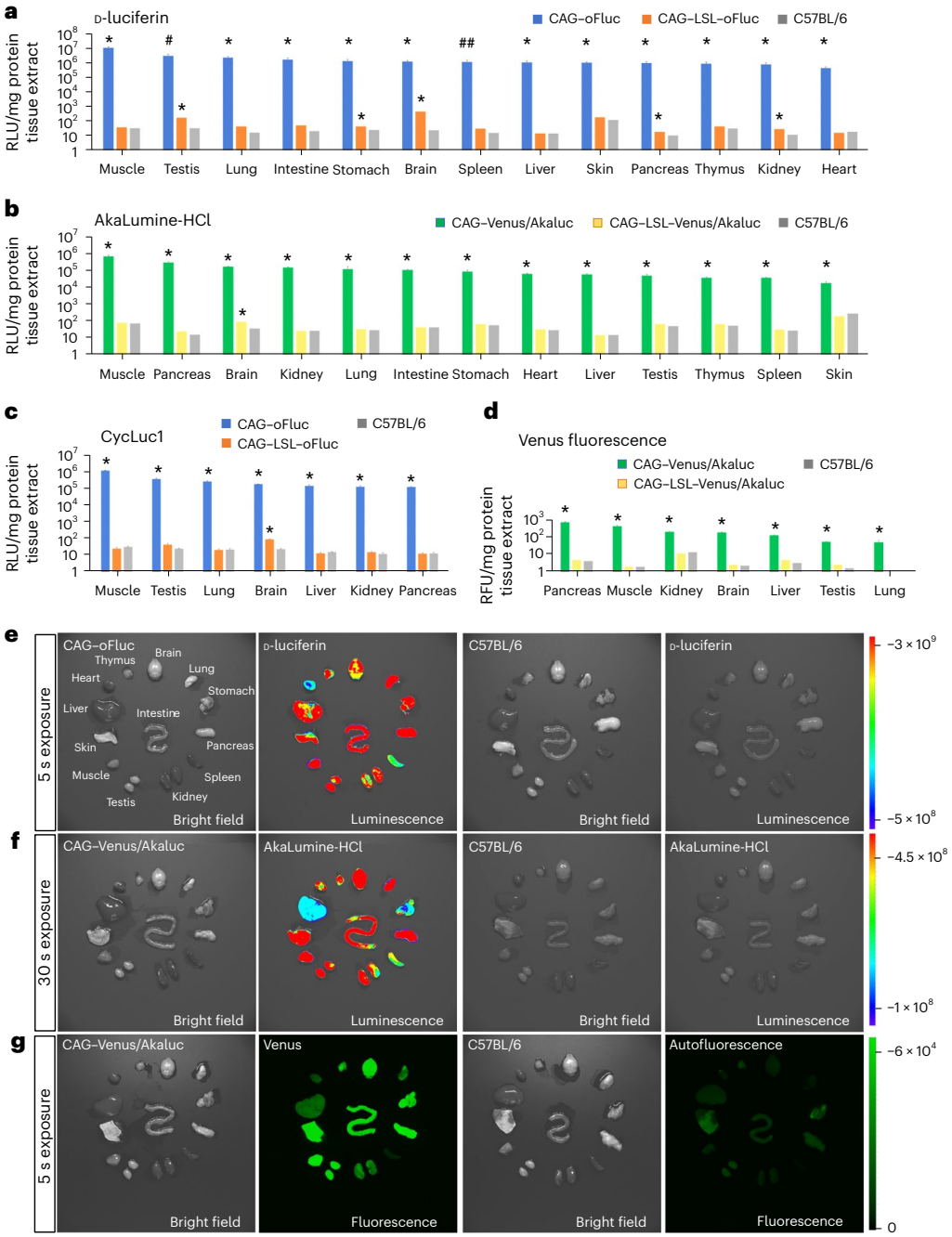

Fig. 2 | Luciferase activity in tissues and their extracts. a,**b**, Relative luminescence units (RLU) normalized to mg of protein tissue extracts of CAG–oFluc (**a**) and CAG–Venus/Akaluc (**b**) mice supplemented with their substrates (1 mM each, D-luciferin and AkaLumine-HCl, respectively). For comparison, tissue extracts were collected before the CAG–Cre cross (that is, CAG–LSL–oFluc and CAG–LSL–Venus/Akaluc) and from C57BL/6 mice, and are included in the graphs. From left to right, tissues exhibiting stronger signals were plotted in order. **c**, RLU of the tissue extracts of oFluc supplemented with 1 mM CycLuc1. **d**, Relative fluorescence units for the Venus reporter in CAG–Venus/Akaluc. $n = 3$ mice per group for tissue extracts. $^{*}P < 0.05$; $^{\#}P = 0.057$; and $^{\#\#}P = 0.059$ compared with C57BL/6 mice (Student's t-test). **e**,**f**, Ex vivo imaging of tissues dissected from CAG–oFluc (**e**) and CAG–Venus/Akaluc (**f**) mice incubated with their substrates (1 mM). As negative controls, tissues from C57BL/6 mice were imaged under the same conditions (right). Scale, photons/s/cm^2/sr. **g**, Ex vivo imaging of Venus fluorescence in tissues from CAG–Venus/Akaluc mice. The images were captured using VISQUE InVivo Smart-LF. Note that C57BL/6 mice exhibited autofluorescence in some tissues when imaged under the same conditions. Scale, intensity (0–65,025).

exposure times, and raw images are presented together for intuitive assessment in Figs. 3 and 4.

For the analysis of nonneural tissues, we used Pdx1–Cre and Lck–Cre mice, which have expression specificities for the pancreas/duodenum[40] or T cells[41], respectively. After crossing with Pdx1–Cre mice (Fig. 3a), the oFluc and Akaluc signals were detectable in the upper abdomen after an exposure of only 5 ms, and were saturated at an exposure of 50 ms or longer. The signal intensities of oFluc and Akaluc were comparable with each other and were sufficiently strong to be captured by a consumer-grade color camera; moreover, their signals could be distinguished on the basis of the emission spectra (Fig. 3c). After crossing with Lck–Cre mice (Fig. 3b), the

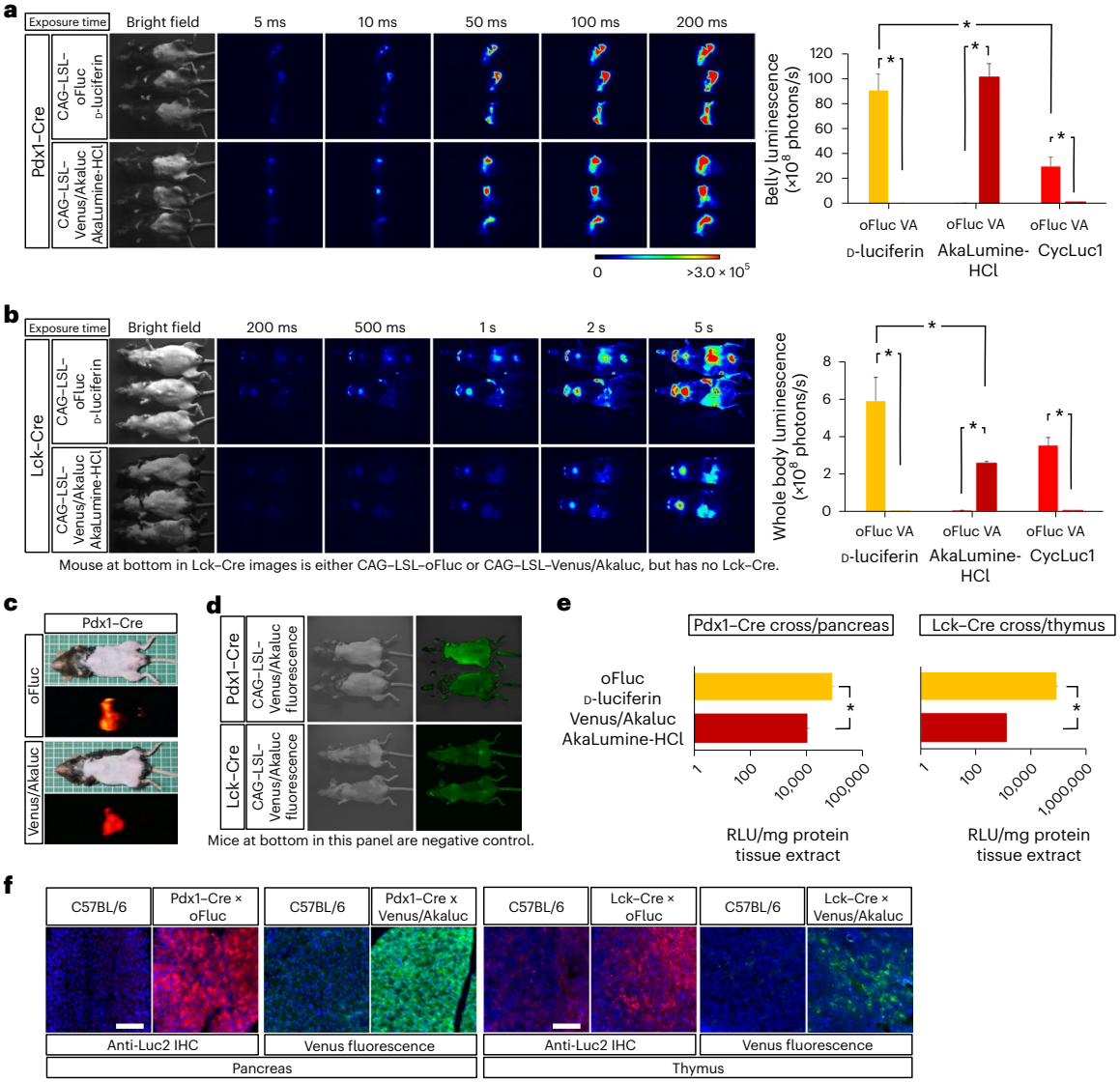

Fig. 3 | In vivo BLI of nonneural tissues. a, In vivo BLI of oFluc and Akaluc in the pancreas by crossing Pdx1-Cre mice with CAG-LSL-oFluc or CAG-LSL-Venus/Akaluc mice. Images were acquired at multiple exposure times. The hair on the lower abdomen of the mice was shaved. Right: quantification of belly luminescence ($n = 5$ each) for three substrates. VA, Venus/Akaluc. $^*P < 0.05$ (Student's t-test). **b**, In vivo BLI of oFluc and Akaluc in T cells by crossing Lck-Cre mice with CAG-LSL-oFluc or CAG-LSL-Venus/Akaluc mice. Note that the signal intensity was relatively weak; therefore, Cre-dependent reporter mice before Cre crossing are included at the bottom of each panel as a negative control. The hair on the abdominal area of the mice was shaved. Scale, photons/s/cm^2. Right: quantification of whole-body luminescence ($n = 5$ each) for three substrates. $^*P < 0.05$ (Student's t-test). **c**, Images captured using a digital color camera. **d**, Venus fluorescence from the experimental mice (top) and negative control mice (bottom) captured by Keyence GFP-lighting system (VB-L12). Note that experimental mice double positive for Cre and Venus/Akaluc were indistinguishable from negative control mice lacking Venus/Akaluc. **e**, RLU of mg protein tissue extracts. oFluc: CAG-LSL-oFluc mice crossed to either Pdx1-Cre or Lck-Cre mice. Venus/Akaluc: CAG-LSL-Venus/Akaluc mice crossed to either Pdx1-Cre or Lck-Cre mice. $^*P < 0.05$ (Student's t-test). **f**, Histological confirmation of reporter expression in the pancreas or thymus using anti-Luc2 IHC (red color) or native Venus fluorescence (green). Counterstained with DAPI (blue). oFluc, CAG-LSL-oFluc mice; Venus/Akaluc, CAG-LSL-Venus/Akaluc mice. Scale bar, 100 μm.

BLI signals appeared to be restricted to the thymus and other lymphoid organs, and oFluc signals were detectable after an exposure of ~200 ms and saturated after an exposure of a few seconds. These signals were apparently generated in a Cre-dependent manner (Fig. 3b, the animals at the bottom of each panel are CAG–LSL–oFluc or CAG–LSL–Venus/Akaluc mice before Cre cross, respectively, and serve as negative controls). Although oFluc produced a much brighter light than Akaluc in thymus extracts incubated with their substrates (Fig. 3e), these differences were greatly attenuated in in vivo BLI, resulting in 2.3-fold stronger signals from oFluc versus Akaluc (Fig. 3b). Histological results confirmed both oFluc and Venus/Akaluc expression in the target tissues (Fig. 3f); however, the target-tissue-specific expression of Venus fluorescence was undetectable from outside the body (Fig. 3d).

We then crossed the reporter strains with Emx1–Cre or Vgat–Cre (also known as Slc32a1–Cre) mice, to visualize the excitatory neurons of the dorsal forebrain[42] or the inhibitory neurons of all neural tissues[43] (Fig. 4). After crossing with Emx1–Cre mice (Fig. 4a), BLI signals were detected in the head, as expected. However, it was surprising to observe the signals in other sites of the body, such as the base

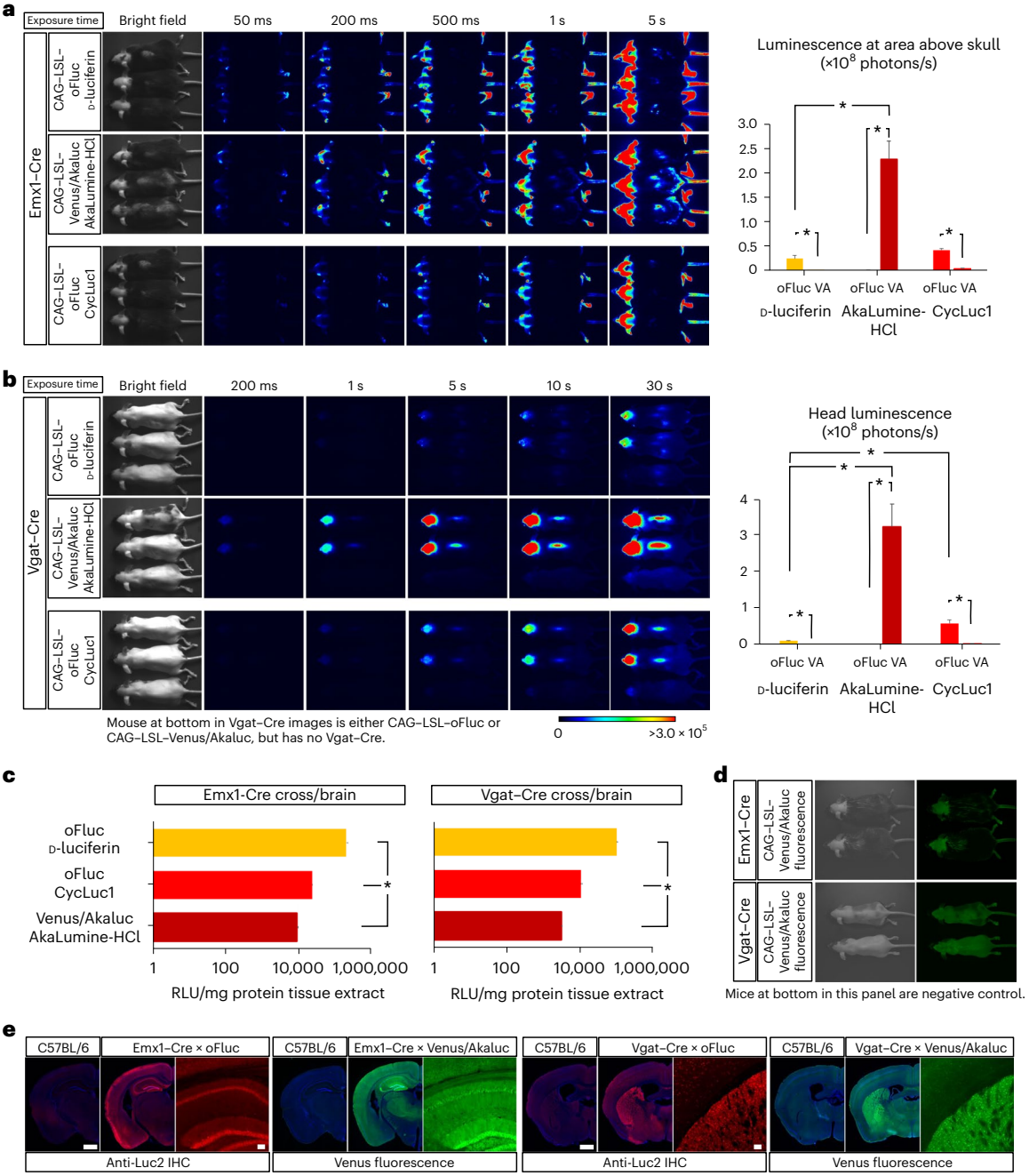

Fig. 4 | In vivo BLI in neural tissues. a, In vivo BLI for oFluc and Akaluc in mice that were double positive for Emx1-Cre and the reporters. Images were acquired at multiple exposure times. The hair of mice in areas of the head and neck was shaved. Right: quantification of luminescence in the area above the skull ($n = 5$ each) for three substrates. VA, Venus/Akaluc. $^*P < 0.05$ (Student's t-test). **b**, In vivo BLI using Vgat-Cre. Note that the signal intensity was relatively weak; therefore, Cre-dependent reporter mice before Cre crossing were included at the bottom of each panel as a negative control. The hair on the dorsal side of the mice was shaved. Scale, photons/s/cm^2. Right: quantification of head luminescence ($n = 5$ each) for three substrates. $^*P < 0.05$ (Student's t-test). **c**, RLU of mg protein tissue extracts. oFluc, CAG-LSL-oFluc mice crossed to either Emx1-Cre or Vgat-Cre mice; Venus/Akaluc, CAG-LSL-Venus/Akaluc mice crossed to either Emx1-Cre or Vgat-Cre mice. $^*P < 0.05$ (Student's t-test) in any of the pairs. **d**, Venus fluorescence of experimental mice (top) and negative control mice (bottom) captured by Keyence GFP-lighting system (VB-L12). The fluorescent signals in experimental mice that were double positive for Cre and Venus/Akaluc were indistinguishable from the autofluorescence obtained in the negative control mice. **e**, Histological confirmation of reporter expression in forebrain sections using anti-Luc2 IHC (red) or native Venus fluorescence (green). Counterstained with DAPI (blue). oFluc, CAG-LSL-oFluc mice; Venus/Akaluc, CAG-LSL-Venus/Akaluc mice. Scale bars, 1 mm for images of whole coronal sections and 100 μm for magnified images.

of the ears, hindlimbs and tail, thus revealing hitherto unknown domains of Cre expression/recombination. After crossing with Vgat–Cre mice (Fig. 4b), the BLI signals were confined to the head and spine, with the latter presumably corresponding to inhibitory neurons in the spinal cord. As predicted from the poor biodistribution of D-luciferin in the brain, a longer exposure time was required to detect oFluc signals through the skull. By contrast, Akaluc signals through the skull could be readily detected within 100–200 ms (the head

luminescence in Akaluc/AkaLumine-HCl mice was 30-fold greater than that detected in oFluc/D-luciferin mice; Fig. 4b, right graph). With CycLuc1 (5 mM, 10 µl per g.b.w.), oFluc signals were greatly increased through the skull (at approximately 5.4-fold over D-luciferin); however, this signal level did not reach to the level achieved by Akaluc (Fig. 4b). Thus, Akaluc/AkaLumine-HCl was the best luciferase/luciferin combination for in vivo BLI in brain tissues. We confirmed oFluc and Venus/Akaluc expression by measuring enzymatic activities in brain tissue extracts and via histological analysis (Fig. 4c,e). None of the Cre crosses yielded Venus fluorescence signals in in vivo imaging (Fig. 4d).

In vivo BLI of CAG–LSL reporter mice before the Cre cross. From the results of the in vitro luciferase assay, we noticed that both CAG–LSL–oFluc and CAG–LSL–Venus/Akaluc mice exhibited very low, albeit significant, luciferase activity in some tissues (Fig. 2a–c). To confirm this observation using in vivo BLI, we performed BLI in both CAG–LSL reporter mice using an EM-CCD camera after the IP injection of the substrates (100 mM D-luciferin, 5 µl per g.b.w.; 15 mM AkaLumine-HCl, 5 µl per g.b.w.; Fig. 5). Using an exposure time of 1 min or longer, oFluc signals appeared around the kidney and testis, whereas Akaluc signals were detected in the head region (Fig. 5a,b). C57BL/6 mice showed no signals. These suspected tissues were consistent with those exhibiting a slight but significant luciferase activity in the tissue extracts (Fig. 2a,b). This finding was further confirmed by ex vivo imaging of the brain and testis (Fig. 5e and Supplementary Fig. 3).

Although the results of the enzymatic assay in the tissue extracts indicated very low but significant luciferase activity in the brains of CAG–LSL–oFluc mice (Fig. 2a), in vivo BLI failed to detect a signal from the heads of these mice (Fig. 5a). We hypothesized that D-luciferin is not delivered efficiently into the brain in vivo compared with AkaLumine-HCl. In fact, ex vivo imaging of dissected brains incubated with their substrates revealed signals in CAG–LSL–oFluc mice (Fig. 5d), similar to CAG–LSL–Venus/Akaluc mice (Fig. 5e). Furthermore, CycLuc1 injection (5 mM, 10 µl per g.b.w.) into CAG–LSL–oFluc improved signal detection in the head (Fig. 5c,f). Thus, although the Cre-dependent mice were initially designed to prevent luciferase expression by the transcription stop cassette, these results indicated that very weak but significant leaky luciferase expression occurred in some tissues. In this sense, BLI was more sensitive than fluorescent imaging, because leaky expression of Venus could not be detected or distinguished from the high background autofluorescence (Fig. 5g).

In vivo dual-color BLI. We designed in vivo dual-color BLI experiments using oFluc and Akaluc in the hope that their emissions would be practically separable (Fig. 1d). We first tested substrate cross-reactivity using recombinant luciferase proteins. We found that both oFluc and Akaluc emitted almost no signal when using their inappropriate substrate (oFluc/AkaLumine and Akaluc/D-luciferin; hereinafter referred to as mismatched pairs) in vitro (Supplementary Fig. 4). We next evaluated the cross-reactivity of substrates in the in vivo setting that used CAG–LSL–oFluc and CAG–LSL–Venus/Akaluc mice individually (Supplementary Figs. 5–8). We confirmed that the original luciferase/substrate pairs (oFluc/D-luciferin and Akaluc/AkaLumine-HCl; hereinafter referred to as matched pairs) produced much stronger signals (more than 88- to 394-fold) than the mismatched pairs (oFluc/AkaLumine-HCl and Akaluc/D-luciferin) (bar graphs in Fig. 3a,b).

Our final challenge was to achieve in vivo dual-color BLI in single mice. To localize both oFluc and Venus/Akaluc deep in the same subject, we generated female mice carrying two types of 'glowing fetuses' (Fig. 6). Fertilized eggs carrying CAG–oFluc and CAG–Venus/Akaluc were collected and transferred separately to the left and right sides, respectively, of the uterus of wild-type mice. We conducted in vivo BLI experiments at the late-gestation stage of E14.5, when fetal positions are largely inferable from the outside (Fig. 6). However, at this stage, the blood–placenta barrier is established[44] and may hinder the intra-fetal biodistribution of D-luciferin. Thus, to redress the concentration balance between the two substrates, we modified the injection doses—doubling the amount of D-luciferin (100 mM, 10 µl per g.b.w.) and reducing the amount of AkaLumine-HCl to 1/5 or 1/10 (3 or 1.5 mM, 5 µl per g.b.w.) relative to the standard doses. The experimental scheme is illustrated in Fig. 6a. After either D-luciferin or AkaLumine-HCl was injected as the first substrate, the side with fetuses with the correct luciferase/luciferin pair began producing a substantial signal, by contrast, the other side did not (Fig. 6b,c, top row), indicating that minimal substrate cross-reactivity occurred in single mice. After injection of the second substrate, we observed that all the transplanted fetuses could glow at both sides comparably in either case (Fig. 6b,c, bottom row).

As the images described above were acquired without any optical filter, no information regarding light wavelengths was obtained. Nevertheless, the difference in emitting colors could be appreciated on the basis of images acquired using the digital color camera (Fig. 6d,e, left half). To separate the oFluc and Akaluc signals spectrally, we used two band-pass (BP) filters, that is, 565 ± 40 BP and 730 ± 45 BP (Supplementary Fig. 9). Although the oFluc/D-luciferin signals leaked slightly into the 730 ± 45 channel (Supplementary Figs. 10 and 11, left uterus imaged with the 730 ± 45 BP filter), the signals of the respective luciferases were effectively separated and sufficiently strong to compose clear merged images (Fig. 6d,e, right half).

Discussion

In the present study, we generated and characterized reporter mouse strains for a new BLI system using the highly bright luciferases oFluc and Akaluc. Akaluc is 100–1,000-fold more sensitive for deep-tissue imaging than the conventional BLI system[26]. oFluc is a novel luciferase that produces at least ten-fold more intense light than the commonly used luciferase (Luc2) in vitro[29]. In the reporter mouse strains, Cre-dependent reporter constructs were knocked into the *ROSA26* locus and driven by the strong *CAG* promoter. After crossing these mice with a Cre-deleter strain, we generated 'glowing mice' that emitted high-intensity light from their entire bodies and tissues. The behavior of these freely moving mice in the dark could be recorded at a video rate of 30 f.p.s. using a consumer-grade digital color camera (Supplementary Movie 1). We also successfully imaged E6.5 embryos in utero using an EM-CCD camera. However, this is probably not the limit of detection; in some cases, E5.5 mouse embryos carrying oFluc could be imaged (data not shown).

The reporter constructs used in this study were designed to be normally silent because of the transcriptional stop signal flanked by loxP sites. The expression of oFluc or Venus/Akaluc is supposed to be induced by the expression of Cre. For example, we achieved deep-tissue imaging of the pancreas, lymphoid organs or specific brain regions by crossing with the appropriate Cre-driver strains (Figs. 3 and 4). Although extremely weak BLI signals were noticed before the Cre crossing, which may be the result of transcriptional leakage, signals that were two orders of magnitude greater were obtained as Cre-dependent signals. Therefore, with an appropriate negative control, true BLI signals can be identified without any difficulty. Interestingly, the leaky expression of Venus/Akaluc was not detected by Venus fluorescence, suggesting low sensitivity of FP imaging in vivo. The results of an enzymatic activity assay in the tissue extracts (Fig. 2) demonstrated that oFluc and Akaluc had wider dynamic ranges (on average, 1.2×10^5-fold and 1.8×10^3-fold, respectively) than Venus (8.5×10-fold).

Two factors are considered for the performance of BLI systems using intact animals. First, the biodistributions of AkaLumine-HCl and D-luciferin differ. D-luciferin was previously used to conduct BLI in the brain[13,45]. However, delivery across the BBB is

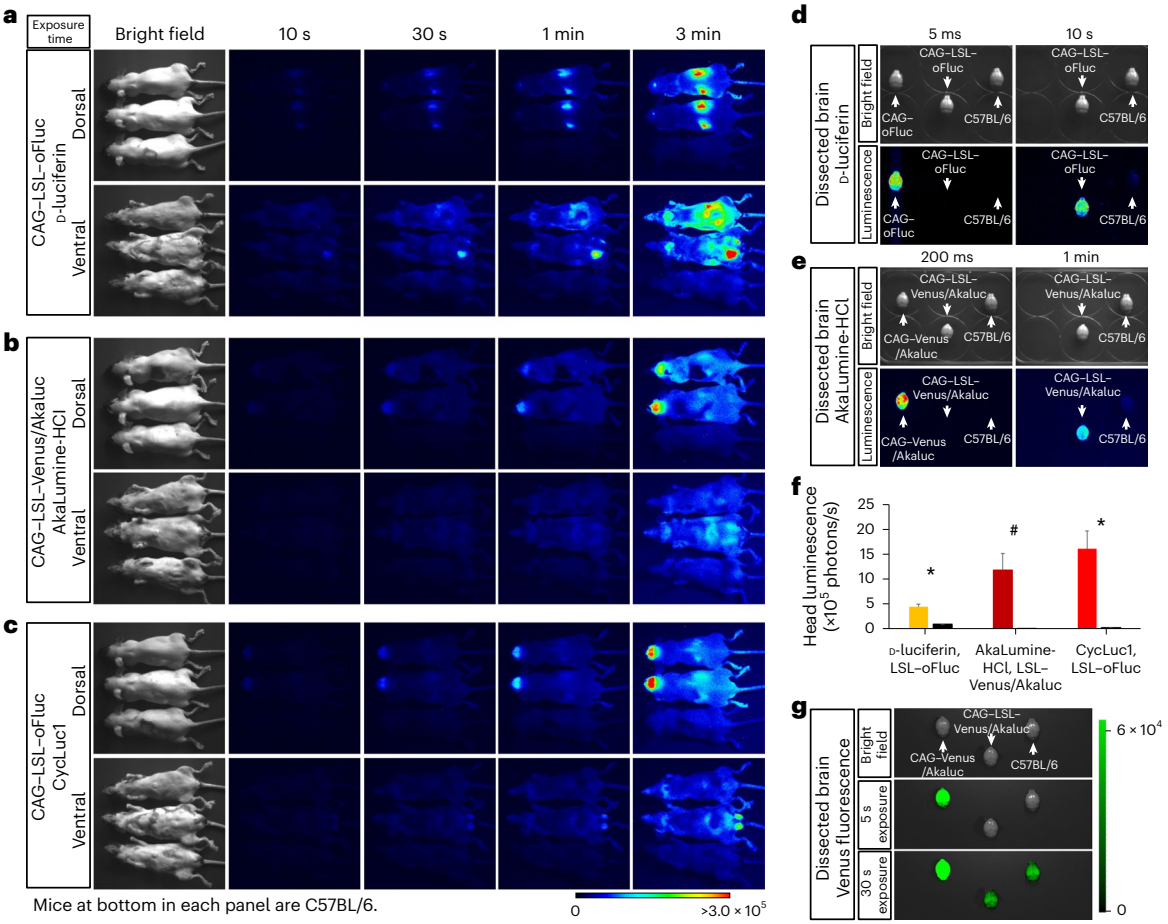

Fig. 5 | In vivo BLI of Cre-dependent reporter mice before the Cre cross. a,**b**, Basal luminescence of CAG–LSL–oFluc (**a**) and CAG–LSL–Venus/Akaluc (**b**) mice at 10 min (dorsal side) and 50 min (ventral side) after IP injection of their substrate (100 mM D-luciferin, 5 µl per g.b.w. for oFluc; 15 mM AkaLumine-HCl, 5 µl per g.b.w. for Akaluc). Images acquired using four different exposure times are shown, and each panel includes three mice (from the top, two experimental mice and a C57BL/6 mouse, as a negative control; mouse sex: female, male and male, respectively). The hair on the dorsal and ventral sides of the mice was shaved. **c**, Basal luminescence of CAG-LSL-oFluc mice after IP injection of CycLuc1 (5 mM, 10 µl per g.b.w.). Images were acquired using the same mice as shown in **a**. Scale, photons/s/cm^2. **d**,**e**, Ex vivo imaging of dissected brains incubated with D-luciferin (1 mM) (**d**) or AkaLumine-HCl (1 mM) (**e**). For longer exposure, the dissected brains of CAG–oFluc or CAG–Venus/Akaluc mice were removed for BLI because their bright luminescence also lit up other tissues, resulting in false-positive signals. **f**, Quantification of head luminescence for in vivo BLI. The black-filled boxes correspond to luminescence in C57BL/6 mice. $n = 4$ for reporter mice and $n = 3$ for C57BL/6 mice. $^*P < 0.05$ and $^\#P = 0.054$ compared with C57BL/6 mice (Student's t-test). **g**, Venus fluorescence imaging using VISQUE InVivo Smart-LF of dissected brains of CAG–Venus/Akaluc, CAG–LSL–Venus/Akaluc and C57BL/6 mice. Scale, intensity (0–65,025).

well achieved with AkaLumine-HCl but not D-luciferin. Thus, the oFluc/D-luciferin system performed poorly in the brain (Fig. 4), although outside the brain, its signals were as bright as or brighter than those of the Akaluc/AkaLumine-HCl system in some cases (Fig. 3). Second, the longer the emission wavelength, the greater the tissue penetration of the light. Although the synthetic luciferin CycLuc1 has improved biodistribution across the BBB[21] and the oFluc/CycLuc1 system produced substantial signals in the brain with a 603 nm emission peak (Fig. 4b), the signal strength could not match that of the Akaluc/AkaLumine-HCl system with a 650 nm emission peak. Taken together, we concluded that the AkaBLI system, composed of Akaluc and AkaLumine-HCl, is the most effective BLI system for detecting luciferase expression in the brain.

The emission peaks of oFluc and Venus/Akaluc are separated by 90 nm (Fig. 1d). The yellow light produced from oFluc is not suitable for in vivo imaging because of its high absorption in the body[4]. However, because of its very high light intensity, the oFluc signal is actually comparable with that of Akaluc in the body, with the exception of the brain (Figs. 3 and 4). These two luciferases have the advantages of high luminosity, sufficiently separated emission peaks, and low cross-reactivity between D-luciferin and AkaLumine-HCl (Fig. 3 and Supplementary Figs. 4–6), rendering them excellent partners for dual-color BLI. For dual-color BLI, an optical filter for the yellow light was selected to detect the oFluc signal. Conversely, because the oFluc signal overlapped partially with the emission spectrum of Venus/Akaluc, which has a peak at 650 nm, we selected an optical filter for the longer side of the shoulder in the emission spectrum of Venus/Akaluc (Supplementary Fig. 9).

Using this setup, it was possible to detect the distinct signals from the two luciferases simultaneously by injecting a single substrate followed by injecting the second substrate (Fig. 6). This administration regimen allowed us to assess substrate cross-reactivity in a single mouse when injecting the first substrate, followed by dual-color imaging after injecting the second substrate. The filter setup used in this experiment effectively separated the signals of the two luciferases; nevertheless, two concerns should be noted. oFluc/D-luciferin produced marginal signals using the longer-wavelength filter (Supplementary Figs. 10 and 11). However, this could be alleviated by the much stronger

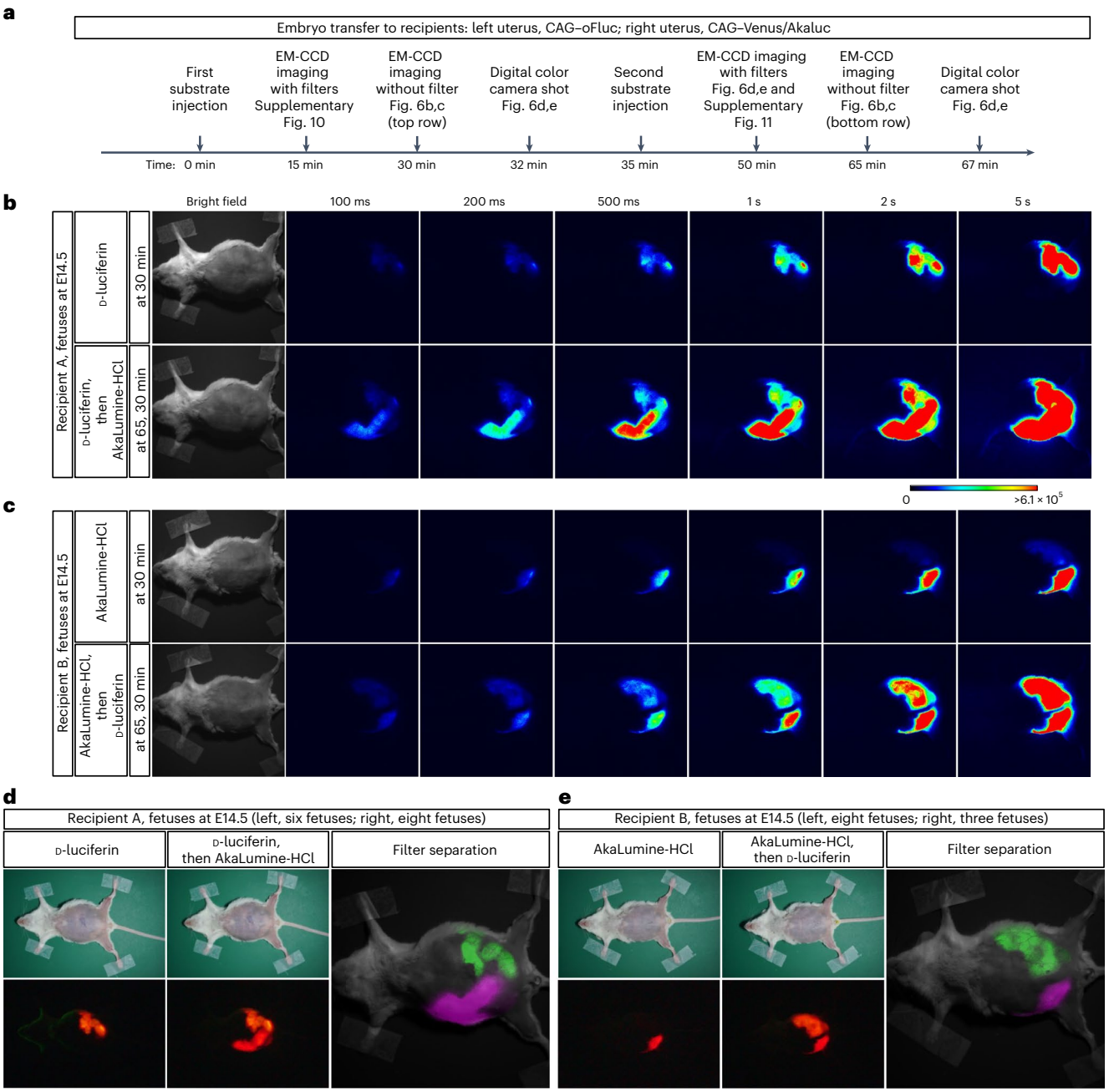

Fig. 6 | In vivo dual-color BLI of 'glowing fetuses' in pregnant mice. Dual-color BLI of recipient mothers transplanted with CAG–oFluc and CAG–Venus/Akaluc embryos into the left and right uteri, respectively. **a**, Timing of substrate injection and imaging. **b**, In vivo BLI without optical filters. Recipient A at 30 min after the injection of the first substrate (top, D-luciferin; 100 mM D-luciferin, 10 µl per g.b.w.) and at 30 min after the injection of the second substrate (bottom, AkaLumine-HCl; 3 mM AkaLumine-HCl, 5 µl per g.b.w.). The first and second substrates were injected sequentially at 35 min intervals; therefore, the images at the bottom were acquired at 65 min after the injection of the first substrate. Number of fetuses in Recipient A: six CAG–oFluc and eight CAG–Venus/Akaluc fetuses in the left and right uteri, respectively. **c**, In vivo BLI without optical filters. Recipient B, in which substrates were injected in the opposite order to that in Recipient A. Number of fetuses in Recipient B: eight CAG–oFluc and three CAG–Venus/Akaluc fetuses in the left and right uteri, respectively. In Recipient B, AkaLumine-HCl was used at a half dose compared with Recipient A. Scale, photons/s/cm^2. **d**,**e**, Images acquired using a digital color camera after the injection of the first (left) or second (middle) substrate. Filter segregation of oFluc and Akaluc (right). After the injection of the second substrate, images were captured by the EM-CCD camera using one of two optical filters (Supplementary Fig. 11). The images were pseudo-colored and merged.

signal intensity of Akaluc/AkaLumine-HCl (Supplementary Figs. 10 and 11). Further characterization of the spectral shifting of signals using a series of filters and the application of spectral unmixing algorithms[46] would improve the separation of signals from the two luciferases. Although we were able to simultaneously detect spectrally distinct signals from the fetuses in the spatially distant locations in the body of pregnant mothers (Fig. 6), future studies are needed to test whether it is possible to discriminate signals in close or overlapping locations in the body using the spectral unmixing algorithm. Inoculation of cells from one of the 'glowing mice' into the other

would be one of the ideal experimental subjects, which should lead to further technical developments of in vivo dual-color BLI in the future. Moreover, because the biodistribution of each substrate may vary within the target tissue in the body, the substrate concentrations to be administered should be carefully determined (empirically).

The availability of two luciferase reporter strains with a comparable signal brightness and distinct emission peaks should facilitate a wide variety of studies in life science fields. For example, behavior of the grafted cell can be traced by in vivo BLI for studies of regenerative medicine[28]. The 'glowing mouse' can be used as an unlimited, reliable and convenient source of luminescent tissues and cells for such transplantation studies. We learned that characteristics of luciferase substrates greatly influence the performance of BLI. Therefore, a variety of mouse strains expressing different luciferase should accelerate studies searching for better luciferin derivatives and evaluating their biodistribution in mice[47–50]. For tissue- and cell-specific labeling using the Cre–loxP system, hundreds of Cre-driver strains have been developed so far, and their specificity has mainly been examined using fluorescent reporter mice[30,51]. Although fluorescent reporters are excellent for the cellular imaging of dissected tissues and sections, screening for specificity at the organismal level is a time-consuming, laborious and often impractical process. However, the BLI systems presented here allow the rapid, unambiguous and noninvasive evaluation of Cre specificity in the whole body. We in fact found that Emx1–Cre × Akaluc mice revealed hitherto unknown domains of the Cre recombination in several body sites other than the brain (Fig. 4a). Once the target sites are narrowed down by in vivo BLI, characterization at cellular resolution can be performed using Venus fluorescence and immunohistochemical detection of luciferase. After confirming the specificity of Cre-driver strains, these strains should offer numerous research tools/materials for noninvasive in vivo BLI, to study various complex biological phenomena in live mice in healthy and diseased conditions.

Online content

Any methods, additional references, Nature Portfolio reporting summaries, source data, extended data, supplementary information, acknowledgements, peer review information; details of author contributions and competing interests; and statements of data and code availability are available at https://doi.org/10.1038/s41684-023-01238-6.

Received: 26 April 2023; Accepted: 1 August 2023;
Published online: 7 September 2023

References

1. Tsien, R. Y. The green fluorescent protein. *Annu. Rev. Biochem.* **67**, 509–544 (1998).
2. Weissleder, R. & Ntziachristos, V. Shedding light onto live molecular targets. *Nat. Med.* **9**, 123–128 (2003).
3. Shaner, N. C., Patterson, G. H. & Davidson, M. W. Advances in fluorescent protein technology. *J. Cell Sci.* **120**, 4247–4260 (2007).
4. Weissleder, R. A clearer vision for in vivo imaging. *Nat. Biotechnol.* **19**, 316–317 (2001).
5. Monici, M. Cell and tissue autofluorescence research and diagnostic applications. *Biotechnol. Annu. Rev.* **11**, 227–256 (2005).
6. Wilson, T. & Hastings, J. W. Bioluminescence. *Annu. Rev. Cell Dev. Biol.* **14**, 197–230 (1998).
7. Contag, C. H. & Bachmann, M. H. Advances in in vivo bioluminescence imaging of gene expression. *Annu. Rev. Biomed. Eng.* **4**, 235–260 (2002).
8. Ogoh, K. et al. Bioluminescence microscopy using a short focal-length imaging lens. *J. Microsc.* **253**, 191–197 (2014).
9. Marjanovic, N. D. et al. Emergence of a high-plasticity cell state during lung cancer evolution. *Cancer Cell* **38**, 229–246 e213 (2020).
10. Palla, A. R. et al. Primary cilia on muscle stem cells are critical to maintain regenerative capacity and are lost during aging. *Nat. Commun.* **13**, 1439 (2022).
11. Tsang, T. et al. Copper is an essential regulator of the autophagic kinases ULK1/2 to drive lung adenocarcinoma. *Nat. Cell Biol.* **22**, 412–424 (2020).
12. Wang, L. et al. Targeting p21(Cip1) highly expressing cells in adipose tissue alleviates insulin resistance in obesity. *Cell Metab.* **34**, 186 (2022).
13. Vooijs, M., Jonkers, J., Lyons, S. & Berns, A. Noninvasive imaging of spontaneous retinoblastoma pathway-dependent tumors in mice. *Cancer Res.* **62**, 1862–1867 (2002).
14. Goeman, F. et al. Molecular imaging of nuclear factor-Y transcriptional activity maps proliferation sites in live animals. *Mol. Biol. Cell* **23**, 1467–1474 (2012).
15. de Latouliere, L. et al. A bioluminescent mouse model of proliferation to highlight early stages of pancreatic cancer: a suitable tool for preclinical studies. *Ann. Anat.* **207**, 2–8 (2016).
16. Manni, I. et al. Monitoring the response of hyperbilirubinemia in the mouse brain by in vivo bioluminescence imaging. *Int. J. Mol. Sci.* **18**, 50 (2016).
17. Manni, I., de Latouliere, L., Gurtner, A. & Piaggio, G. Transgenic animal models to visualize cancer-related cellular processes by bioluminescence imaging. *Front. Pharmacol.* **10**, 235 (2019).
18. Lee, K. H. et al. Cell uptake and tissue distribution of radioiodine labelled D-luciferin: implications for luciferase based gene imaging. *Nucl. Med. Commun.* **24**, 1003–1009 (2003).
19. Berger, F., Paulmurugan, R., Bhaumik, S. & Gambhir, S. S. Uptake kinetics and biodistribution of 14C-D-luciferin—a radiolabeled substrate for the firefly luciferase catalyzed bioluminescence reaction: impact on bioluminescence based reporter gene imaging. *Eur. J. Nucl. Med. Mol. Imaging* **35**, 2275–2285 (2008).
20. Kuchimaru, T. et al. A luciferin analogue generating near-infrared bioluminescence achieves highly sensitive deep-tissue imaging. *Nat. Commun.* **7**, 11856 (2016).
21. Evans, M. S. et al. A synthetic luciferin improves bioluminescence imaging in live mice. *Nat. Methods* **11**, 393–395 (2014).
22. Branchini, B. R. et al. Red-emitting luciferases for bioluminescence reporter and imaging applications. *Anal. Biochem.* **396**, 290–297 (2010).
23. Liang, Y., Walczak, P. & Bulte, J. W. Comparison of red-shifted firefly luciferase Ppy RE9 and conventional Luc2 as bioluminescence imaging reporter genes for in vivo imaging of stem cells. *J. Biomed. Opt.* **17**, 016004 (2012).
24. Mezzanotte, L. et al. Evaluating reporter genes of different luciferases for optimized in vivo bioluminescence imaging of transplanted neural stem cells in the brain. *Contrast Media Mol. Imaging* **8**, 505–513 (2013).
25. Zambito, G. et al. Evaluating brightness and spectral properties of click beetle and firefly luciferases using luciferin analogues: identification of preferred pairings of luciferase and substrate for in vivo bioluminescence imaging. *Mol. Imaging Biol.* **22**, 1523–1531 (2020).
26. Iwano, S. et al. Single-cell bioluminescence imaging of deep tissue in freely moving animals. *Science* **359**, 935–939 (2018).
27. Mezzanotte, L. et al. Sensitive dual color in vivo bioluminescence imaging using a new red codon optimized firefly luciferase and a green click beetle luciferase. *PLoS ONE* **6**, e19277 (2011).
28. Ago, K. et al. A non-invasive system to monitor in vivo neural graft activity after spinal cord injury. *Commun. Biol.* **5**, 803 (2022).
29. Ogoh, K., Akiyoshi, R. & Suzuki, H. Cloning and mutagenetic modification of the firefly luciferase gene and its use for bioluminescence microscopy of engrailed expression during *Drosophila* metamorphosis. *Biochem. Biophys. Rep.* **23**, 100771 (2020).
30. Madisen, L. et al. A robust and high-throughput Cre reporting and characterization system for the whole mouse brain. *Nat. Neurosci.* **13**, 133–140 (2010).
31. Safran, M. et al. Mouse reporter strain for noninvasive bioluminescent imaging of cells that have undergone Cre-mediated recombination. *Mol. Imaging* **2**, 297–302 (2003).
32. Woolfenden, S., Zhu, H. & Charest, A. A Cre/LoxP conditional luciferase reporter transgenic mouse for bioluminescence monitoring of tumorigenesis. *Genesis* **47**, 659–666 (2009).
33. Ishikawa, T. O. & Herschman, H. R. Conditional bicistronic Cre reporter line expressing both firefly luciferase and β-galactosidase. *Mol. Imaging Biol.* **13**, 284–292 (2011).
34. Hara-Miyauchi, C. et al. Bioluminescent system for dynamic imaging of cell and animal behavior. *Biochem. Biophys. Res. Commun.* **419**, 188–193 (2012).
35. Niwa, H., Yamamura, K. & Miyazaki, J. Efficient selection for high-expression transfectants with a novel eukaryotic vector. *Gene* **108**, 193–199 (1991).
36. Zufferey, R., Donello, J. E., Trono, D. & Hope, T. J. Woodchuck hepatitis virus posttranscriptional regulatory element enhances expression of transgenes delivered by retroviral vectors. *J. Virol.* **73**, 2886–2892 (1999).
37. Nagai, T. et al. A variant of yellow fluorescent protein with fast and efficient maturation for cell-biological applications. *Nat. Biotechnol.* **20**, 87–90 (2002).
38. Sakai, K. & Miyazaki, J. A transgenic mouse line that retains Cre recombinase activity in mature oocytes irrespective of the Cre transgene transmission. *Biochem. Biophys. Res. Commun.* **237**, 318–324 (1997).
39. Nagy, A. *Manipulating the Mouse Embryo: A Laboratory Manual* (Cold Spring Harbor Laboratory Press, 2003).

40. Shibata, H. et al. In vivo reprogramming drives Kras-induced cancer development. *Nat. Commun.* **9**, 2081 (2018).
41. Takahama, Y. et al. Functional competence of T cells in the absence of glycosylphosphatidylinositol-anchored proteins caused by T cell-specific disruption of the Pig-a gene. *Eur. J. Immunol.* **28**, 2159–2166 (1998).
42. Iwasato, T. et al. Cortex-restricted disruption of NMDAR1 impairs neuronal patterns in the barrel cortex. *Nature* **406**, 726–731 (2000).
43. Ogiwara, I. et al. Nav1.1 haploinsufficiency in excitatory neurons ameliorates seizure-associated sudden death in a mouse model of Dravet syndrome. *Hum. Mol. Genet.* **22**, 4784–4804 (2013).
44. Watson, E. D. & Cross, J. C. Development of structures and transport functions in the mouse placenta. *Physiology* **20**, 180–193 (2005).
45. Uhrbom, L., Nerio, E. & Holland, E. C. Dissecting tumor maintenance requirements using bioluminescence imaging of cell proliferation in a mouse glioma model. *Nat. Med.* **10**, 1257–1260 (2004).
46. Xu, H. & Rice, B. W. In-vivo fluorescence imaging with a multivariate curve resolution spectral unmixing technique. *J. Biomed. Opt.* **14**, 064011 (2009).
47. Stowe, C. L. et al. Near-infrared dual bioluminescence imaging in mouse models of cancer using infraluciferin. *eLife* **8**, e45801 (2019).
48. Ikeda, Y., Nomoto, T., Hiruta, Y., Nishiyama, N. & Citterio, D. Ring-fused firefly luciferins: expanded palette of near-infrared emitting bioluminescent substrates. *Anal. Chem.* **92**, 4235–4243 (2020).
49. Ji, X., Adams, S. T. Jr & Miller, S. C. Bioluminescence imaging in mice with synthetic luciferin analogues. *Methods Enzymol.* **640**, 165–183 (2020).
50. Saito-Moriya, R. et al. How to select firefly luciferin analogues for in vivo imaging. *Int. J. Mol. Sci.* **22**, 1848 (2021).
51. Daigle, T. L. et al. A suite of transgenic driver and reporter mouse lines with enhanced brain-cell-type targeting and functionality. *Cell* **174**, 465–480 e422 (2018).

Publisher's note Springer Nature remains neutral with regard to jurisdictional claims in published maps and institutional affiliations.

Open Access This article is licensed under a Creative Commons Attribution 4.0 International License, which permits use, sharing, adaptation, distribution and reproduction in any medium or format, as long as you give appropriate credit to the original author(s) and the source, provide a link to the Creative Commons license, and indicate if changes were made. The images or other third party material in this article are included in the article's Creative Commons license, unless indicated otherwise in a credit line to the material. If material is not included in the article's Creative Commons license and your intended use is not permitted by statutory regulation or exceeds the permitted use, you will need to obtain permission directly from the copyright holder. To view a copy of this license, visit http://creativecommons.org/licenses/by/4.0/.

© The Author(s) 2023

Methods

Ethical statements. All experimental protocols and husbandry for mice were approved by the Institutional Animal Care and Use Committee of RIKEN Tsukuba Branch and University of Tsukuba, and all mice were cared for and treated humanely in accordance with the Committee's guiding principles.

Construction of targeting vectors. Targeting vectors were constructed on the basis of a plasmid described in a previous study[52]. They comprised the homology arms—1.1 kb at the 5′ portion and 2.8 kb at the 3′ portion—of the *ROSA26* locus, and an insert DNA fragment including the *CAG* promoter followed by a pair of loxP sites flanking the neomycin resistance gene (*Neo*) and SV40 poly A (which were derived from pCALNL5 (RDB01862)), followed by either the luciferase derived from *Pyrocoeli matsumurai* (oFluc, RDB14359) or Venus/Akaluc (RDB15781), with the addition of a WPRE and bovine growth hormone ploy A at the 3′ end. The resulting insert DNA fragment of oFluc was ligated to the XbaI site of the *ROSA26* homology arm, whereas that of Venus/Akaluc was ligated to the *ROSA26* homology arm, with parts of the arms being deleted—94 bp upstream and 41 bp downstream of the XbaI site—to increase guide RNA (gRNA) selection for CRISPR-Cas9 genome editing.

Generation of mouse strains. Mice were generated using the CRISPR-Cas9 technique with zygotes derived from C57BL/6JCrl mice, as described in a previous study[53]. The target sequences of gRNAs in the *ROSA26* locus were as follows: 5′–CGCCCATCTTCTAGAAAGAC–3′ for oFluc and 5′–TGGCTTCTGAGGACCGCCCT–3′ for Venus/Akaluc. Cas9, gRNA and the targeting vector were microinjected in the form of nonlinearized plasmid DNAs, and then pups born after zygote implantation into the oviducts of foster mothers were screened by polymerase chain reaction (PCR). An initial screening was carried out to confirm homologous recombination targeting the *ROSA26* locus using PCR primers that annealed to the genomic region external to the homology arms and the insert DNA fragment corresponding to *CAG* or WPRE for the 5′ and 3′ regions, respectively. The integration of the plasmid backbone of the targeting vector was also tested using PCR primers that detected the ampicillin-resistance gene. These primer sets are listed in Supplementary Table 1. Founder mice were selected on the basis of 5′ and 3′ homologous recombination at the *ROSA26* locus, regardless of the presence of the plasmid backbone. The founder mice were further bred with C57BL/6JCrl mice.

Evaluation of targeted knock-in in germ-line-transmitted mouse lines. The genotypes of N1 pups from founder mice were tested using the PCR primers described in the previous section. To assess the genomic structure, further PCR was conducted using additional primers that could amplify the plasmid backbone used in the targeting vectors. In addition, the copy number of the insert DNA fragment integrated into the mouse genome was determined by quantitative PCR with separate amplification of two components—*Neo* and WPRE; their copy number was compared with a standard genomic DNA (RBRC04874) that was previously confirmed to represent the integration of one copy into the *ROSA26* locus[52]. Targeted knock-in was evaluated in mice after the CAG–Cre cross, as described above. Furthermore, the absence of floxed *Neo* was tested using two primer sets, one for *Neo* and the other for the regions upstream and downstream of *Neo*. The primers used in this section are listed in Supplementary Table 1.

Animal breeding. All mice were provided with commercial laboratory mouse diet and water ad libitum, and were housed under lighting conditions (light on from 8:00 to 20:00) and specific pathogen-free conditions. The Cre-driver mice used in this study were as follows: C57BL/6-Tg(CAG-cre)13Miya (RBRC09807, CAG–Cre), B6.129P2-Emx1$^{tm1.1(cre)Ito}$/ItoRbrc (RBRC01345, Emx1–Cre), C57BL/6J-Tg(Slc32a1-cre)65Kzy (RBRC10606, Vgat–Cre), B6;Cg-Pdx1$^{tm1(cre)Yasu}$ (RBRC10170, Pdx1–Cre), and B6.Cg-Tg(Lck-cre)1Jtak (RBRC04738, Lck–Cre). All of these Cre-driver mice were obtained from RIKEN BRC. In general, male Cre-driver mice were bred with female reporter mice to generate compound Cre- and reporter-positive mice. CAG–LSL–oFluc and CAG–LSL–Venus/Akaluc mice were crossed with CAG–Cre mice to generate CAG–oFluc and CAG–Venus/Akaluc mice, respectively, in which DNA fragments between loxP sites (between the most distant loxP pairs in the case of CAG–LSL–oFluc mice) were removed in the germline. As a result, oFluc and Venus/Akaluc protein expression was driven by the CAG promoter. B6.Cg-c/c Hr^{hr} (RBRC05798) mice were used to introduce the albino and/or hairless phenotype only when bioluminescent imaging was conducted in freely behaving mice. All mouse strains and their genotyping protocols are available from RIKEN BRC at https://mus.brc.riken.jp/en/. For in vivo imaging of pregnant females carrying E6.5 embryos, BALB/c mice were purchased from CLEA Japan and crossed with CAG–oFluc or CAG–Venus/Akaluc mice. Some of their pups were imaged at postnatal day 4.

Evaluation of luciferase enzymatic activity and of the fluorescence intensity of crude tissue extracts. Mice were killed via cervical dislocation, and their tissues were immediately dissected, snap-frozen in liquid nitrogen, and stored at −80 °C until use. The frozen tissues (50–250 mg) were lysed with a 5× volume of lysis buffer containing 25 mM Tris/phosphate, 4 mM ethylene glycol-bis (2-aminoethylether)-*N*,*N*,*N*′,*N*′-tetraacetic acid (EGTA), 1% Triton X-100, 10% glycerol, 2 mM dithiothreitol and an ethylenediaminetetraacetic acid-free protease inhibitor cocktail (Roche), followed by homogenization with zirconia beads in a refrigerated Micro Smash MS-100R instrument (TOMY) for 30 s twice. After brief centrifugation, the supernatants were transferred to clean tubes and their protein concentrations were measured using a BCA Protein Assay Kit (Pierce Thermo Scientific), according to the manufacturer's instructions. Subsequently, 20 µl of the supernatant was mixed with 180 µl of the assay buffer containing 25 mM Tris/phosphate, 20 mM $MgSO_4$, 4 mM EGTA, 2 mM ATP, 1 mM dithiothreitol and 1 mM substrate in a black-walled 96-well plate (Thermo Fisher Scientific), and then immediately measured on a luminometer (BioTek Synergy HTX, Agilent Technologies). The values of bioluminescence recorded at 5 min after mixing were compared among genotypes. Stock solutions of the three substrates, that is, D-luciferin (Cayman Chemical Company), AkaLumine-HCl (Wako) and CycLuc1 (MedChemExpress), were dissolved in phosphate-buffered saline (PBS), distilled water, and PBS at final concentrations of 100, 100 and 5 mM, respectively. In addition, the fluorescence intensity of Venus/Akaluc was measured using a BioTek Synergy HTX reader.

Measurement of the emission spectra of recombinant oFluc and Venus/Akaluc. The cDNA of either oFluc (RDB14359 from RIKEN BRC) or Venus/Akaluc[26] was inserted in the multiple cloning site of pRSET-B using BamHI and EcoRI (Thermo Fisher Scientific). The luciferase protein expressed in NiCo21(DE3) competent *Escherichia coli* (New England Biolabs) was purified using a Ni-NTA agarose resin column (Qiagen) and a chitin resin column (New England Biolabs). Protein concentrations were measured using a Bradford Protein Assay (Bio-Rad). Emission spectra were determined using a LumiFl-Spectrocapture AB-1850 instrument (Atto) at 37 °C in a solution of 0.1 M citrate phosphate buffer (pH 7.0) containing the substrate (1 mM D-luciferin or 10 µM AkaLumine), 1 mM ATP, 2 mM $MgSO_4$ and each of the purified luciferases (10 ng/µl in 100 µl reaction volume).

Measurement of the Michaelis–Menten constant (K_m) values. K_m for oFluc or Venus/Akaluc for D-luciferin or AkaLumine were determined with a luminometer, Nivo S (PerkinElmer). Luminescence intensity was measured in 0.1 M citric acid/0.1 M Na_2HPO_4 buffer (pH 7.0) containing 2 µg/µl of partially purified luciferase, 1 mM ATP, 2 mM $MgSO_4$ and luciferin (D-luciferin 0–990 µM, AkaLumine 0–208 µM). The time course of light emission was measured for 10 s. The K_m was estimated by curve fitting against the Michaelis–Menten equation.

Ex vivo BLI. Tissues were isolated immediately after the cervical dislocation of mice and the dissected tissues were incubated in PBS containing 1 mM substrate for 5 min. Subsequently, BLI signals were captured with VISQUE InVivo Smart-LF (Vieworks) and analyzed using the accompanying software, CleVue. The fluorescence signals were also imaged with InVivo Smart-LF. Dissected brains and testes (Fig. 5 and Supplementary Fig. 3) were imaged with an ImagEM 9100-13 (Hamamatsu Photonics) and a lens (#903018, AstroScope) set up in a dark chamber, and the acquired images were analyzed using CellSense software (Olympus). The signal intensities captured by ImagEM 9100-13 were calibrated using KoshiUni (Atto), to determine its sensitivity, and are presented as the absolute photon number per second and cm^2.

In vivo BLI. Before the imaging session, any hair covering the region of interest was removed using a shaver followed by depilatory cream. Mice were anesthetized with a combination of anesthetics, as follows: 0.3 mg/kg medetomidine, 4.0 mg/kg midazolam, and 5.0 mg/kg butorphanol. Bioluminescence images were acquired with an ImagEM 9100-13 (Hamamatsu Photonics) and a lens (#903018, AstroScope) set up in a dark chamber. In each imaging session, one of three substrates was injected intraperitoneally at the dose indicated in Results in proportion to the g.b.w. of mice, and image acquisition generally started 10 min after substrate administration at multiple exposure times. The images were analyzed using CellSense software. Movies of freely behaving mice were recorded using a digital color camera, α7SII, with the following settings: ISO, 102400; f2.9 lens (Sony) in a dark room. For successive imaging sessions using multiple substrates, each imaging session was separated by at least 24 h and the absence of the luminescence signal emitted from the previous imaging session was confirmed at the beginning of each new imaging session. Data from images acquired by an ImagEM 9100-13 were quantified using ImageJ software (NIH) based on the calibration data provided by KoshiUni (Atto). Fluorescence images were also acquired using a VISQUE InVivo Smart-LF or Keyence GFP-lighting system (VB-L12, Keyence) equipped with a CCD camera (DFC450C, Leica Microsystems).

Histology. The dissected tissues were fixed with 4% paraformaldehyde in 0.1 M phosphate buffer overnight, and then embedded in optimal cutting temperature (OCT) compound (Sakura). The tissues were further treated with 30% sucrose overnight. Cryostat sections were prepared for native fluorescence imaging and anti-Luc2 (MBL) immunohistochemistry (IHC). For anti-Luc2 IHC, the tissue sections were first blocked with PBS containing 3% normal donkey serum and 0.3% Triton X-100, and then incubated with a rabbit anti-Luc2 antibody (1,000× dilution) overnight at 18 °C. After washing three times with PBS, the sections were further incubated with ImmPRESS (Vectorlabs) for 2 h at 24 °C. Signals were

visualized with TSA-Cy3 (PerkinElmer). All sections were counterstained with 4′,6-diamidino-2-phenylindole (DAPI; Thermo Fisher Scientific).

In vivo dual-color BLI. Heterozygous fertilized eggs were prepared via in vitro fertilization using sperm from homozygous males of either the CAG–oFluc or CAG–Venus/Akaluc strains and eggs of C57BL/6. In vivo dual-color BLI was conducted with two Institute of Cancer Research (ICR) recipients (CLEA Japan) in which heterozygous CAG–oFluc embryos had been transferred into the left uteri and heterozygous CAG–Vensu/Akaluc embryos into the right uteri. Bioluminescence images were acquired with an ImagEM 9100-13 (Hamamatsu Photonics) and a lens (HF25HA-1B, Fujinon), without any filter, which were set up in a dark chamber. Images were further acquired using two BP filters (565 ± 40 BP and 730 ± 45 BP from Omega Optical) attached to the lens sequentially to separate the signals from oFluc and Venus/Akaluc. Substrate dosage and the timing of their injection and imaging are described in Results and Fig. 6a.

Statistical analysis. All data are presented as the mean ± standard error of the mean. Data between groups were compared using a Student's *t*-test. The null hypothesis was rejected at the $P < 0.05$ level.

Reporting summary. Further information on research design is available in the Nature Portfolio Reporting Summary linked to this article.

Data availability

The data that support the findings of this study are available from the corresponding author upon request. Luciferase reporter mice generated in this study were deposited at RIKEN BioReource Research Center under the following registration numbers and strain names. CAG–LSL–oFluc mice: RBRC 10451 C57BL/6J-Gt(ROSA)26Sor$^{em13(CAG\text{-}luc)Rbrc}$/#77. CAG–LSL–Venus/Akaluc mice: RBRC10858 C57BL/6J-Gt(ROSA)26Sor$^{em14(CAG\text{-}Venus/Akaluc)Rbrc}$/#87. CAG–oFluc mice: RBRC10919 C57BL/6J-Gt(ROSA)26Sor$^{em13.1(CAG\text{-}luc)Rbrc}$/#77. CAG–Venus/Akaluc mice: RBRC10921 C57BL/6J-Gt(ROSA)26Sor$^{em17.1(CAG\text{-}Venus/Akaluc)Rbrc}$/#11. Source data are provided with this paper.

References

52. Hasegawa, Y. et al. Novel ROSA26 Cre-reporter knock-in C57BL/6N mice exhibiting green emission before and red emission after Cre-mediated recombination. *Exp. Anim.* **62**, 295–304 (2013).

53. Mizuno-Iijima, S. et al. Efficient production of large deletion and gene fragment knock-in mice mediated by genome editing with Cas9-mouse Cdt1 in mouse zygotes. *Methods* **191**, 23–31 (2021).

Acknowledgements

We thank J. Miyazaki, S. Itohara, Y. Yamada, J. Takeda and K. Ochiai for their generous deposition of mouse strains in the RIKEN BRC and for allowing their use in this study. We also thank the members of the Experimental Animal Division of RIKEN BRC, especially M. Kadota, Y. Yamashita and K. Otaka, for their excellent technical assistance, and M. Sugimoto for his help with embryo imaging. This work was supported by JSPS KAKENHI grant no. JP26890026 to T.N., and in part by JST grant no. JPMJPF1234 to A.Y. The project was also supported in part by the RIKEN BRC director's discretionary fund.

Author contributions

T.N. conceived, designed and performed all the experiments (except for the emission spectra of recombinant proteins), analyzed all data and drafted the manuscript. K.O. conceived, designed and performed the experiment to measure the emission spectra. S.I. conceived the project and provided critical input on this study. T.S. conceived and supported the entire project, especially regarding the imaging setup. S.M.-I. conducted the initial screening of founder mice. K.N. conducted the initial screening of founder mice. S.M. and F.S. generated founder mice. A.Y. managed the animal facility and secured funding. A.M. conceived the project, provided critical input on this study and edited the manuscript. K.A. conceived and supervised the project, and drafted the manuscript.

Competing interests

The authors declare no competing interests.

Additional information

Supplementary information The online version contains supplementary material available at https://doi.org/10.1038/s41684-023-01238-6.

Correspondence and requests for materials should be addressed to Toshiaki Nakashiba.

Peer review information *Lab Animal* thanks Giulia Piaggio and the other, anonymous, reviewer(s) for their contribution to the peer review of this work.

Reprints and permissions information is available at www.nature.com/reprints.

nature portfolio

Corresponding author(s): Toshiaki Nakashiba

Last updated by author(s): Jul 13, 2023

Reporting Summary

Nature Portfolio wishes to improve the reproducibility of the work that we publish. This form provides structure for consistency and transparency in reporting. For further information on Nature Portfolio policies, see our Editorial Policies and the Editorial Policy Checklist.

Statistics

For all statistical analyses, confirm that the following items are present in the figure legend, table legend, main text, or Methods section.

n/a	Confirmed
☐	☒ The exact sample size (*n*) for each experimental group/condition, given as a discrete number and unit of measurement
☐	☒ A statement on whether measurements were taken from distinct samples or whether the same sample was measured repeatedly
☐	☒ The statistical test(s) used AND whether they are one- or two-sided *Only common tests should be described solely by name; describe more complex techniques in the Methods section.*
☒	☐ A description of all covariates tested
☐	☒ A description of any assumptions or corrections, such as tests of normality and adjustment for multiple comparisons
☐	☒ A full description of the statistical parameters including central tendency (e.g. means) or other basic estimates (e.g. regression coefficient) AND variation (e.g. standard deviation) or associated estimates of uncertainty (e.g. confidence intervals)
☐	☒ For null hypothesis testing, the test statistic (e.g. *F*, *t*, *r*) with confidence intervals, effect sizes, degrees of freedom and *P* value noted *Give P values as exact values whenever suitable.*
☒	☐ For Bayesian analysis, information on the choice of priors and Markov chain Monte Carlo settings
☒	☐ For hierarchical and complex designs, identification of the appropriate level for tests and full reporting of outcomes
☒	☐ Estimates of effect sizes (e.g. Cohen's *d*, Pearson's *r*), indicating how they were calculated

Our web collection on statistics for biologists contains articles on many of the points above.

Software and code

Policy information about availability of computer code

Data collection	BioTek Synergy HTX (Agilent Technologies, CA, USA) for tissue extract assays. LumiFl-Spectrocapture AB-1850 instrument (Atto, Tokyo, Japan) for measurement of the emission spectra. Nivo S (PerkinElmer, MA, USA) for measurement of the Km values. VISQUE InVivo Smart-LF (Vieworks, Gyeonggi-do, Korea) for ex vivo imaging. ImagEM 9100-13 (Hamamatsu Photonics, Shizuoka, Japan) for in vivo imaging. Keyence GFP-lighting system (VB-L12, Keyence, Osaka, Japan) for GFP whole body imaging. alpha-7SII digital color camera (Sony, Japan) for real time imaging of live mice.
Data analysis	CellSense software (Olympus,Tokyo, Japan), ImageJ software (version 1.53a, NIH) and CleVue (Vieworks, Gyeonggi-do, Korea) were used for data analysis.

For manuscripts utilizing custom algorithms or software that are central to the research but not yet described in published literature, software must be made available to editors and reviewers. We strongly encourage code deposition in a community repository (e.g. GitHub). See the Nature Portfolio guidelines for submitting code & software for further information.

Data

Policy information about availability of data

All manuscripts must include a data availability statement. This statement should provide the following information, where applicable:

- Accession codes, unique identifiers, or web links for publicly available datasets
- A description of any restrictions on data availability
- For clinical datasets or third party data, please ensure that the statement adheres to our policy

The data obtained from this study are available from the corresponding author upon reasonable request.

Human research participants

Policy information about studies involving human research participants and Sex and Gender in Research.

Reporting on sex and gender	No human research participants in this study.
Population characteristics	*Describe the covariate-relevant population characteristics of the human research participants (e.g. age, genotypic information, past and current diagnosis and treatment categories). If you filled out the behavioural & social sciences study design questions and have nothing to add here, write "See above."*
Recruitment	*Describe how participants were recruited. Outline any potential self-selection bias or other biases that may be present and how these are likely to impact results.*
Ethics oversight	*Identify the organization(s) that approved the study protocol.*

Note that full information on the approval of the study protocol must also be provided in the manuscript.

Field-specific reporting

Please select the one below that is the best fit for your research. If you are not sure, read the appropriate sections before making your selection.

☒ Life sciences ☐ Behavioural & social sciences ☐ Ecological, evolutionary & environmental sciences

For a reference copy of the document with all sections, see nature.com/documents/nr-reporting-summary-flat.pdf

Life sciences study design

All studies must disclose on these points even when the disclosure is negative.

Sample size	Statistical methods were not used a priori to determine the sample sizes. The sample sizes used in this study are similar to those widely used in this field.
Data exclusions	No data exclusions in this study.
Replication	All studies were repeated at least twice with similar results.
Randomization	No randomization was applied in this study.
Blinding	No blinding was applied in this study.

Reporting for specific materials, systems and methods

We require information from authors about some types of materials, experimental systems and methods used in many studies. Here, indicate whether each material, system or method listed is relevant to your study. If you are not sure if a list item applies to your research, read the appropriate section before selecting a response.

Materials & experimental systems

n/a	Involved in the study
☐	☒ Antibodies
☒	☐ Eukaryotic cell lines
☒	☐ Palaeontology and archaeology
☐	☒ Animals and other organisms
☒	☐ Clinical data
☒	☐ Dual use research of concern

Methods

n/a	Involved in the study
☒	☐ ChIP-seq
☒	☐ Flow cytometry
☒	☐ MRI-based neuroimaging

Antibodies

Antibodies used	rabbit anti-Luc2 (catlogu number: PM016, MBL, Tokyo, Japan)
Validation	According to the websites of MBL, this antibody has been validated by at least 3 literatures.

Animals and other research organisms

Policy information about studies involving animals; ARRIVE guidelines recommended for reporting animal research, and Sex and Gender in Research

Laboratory animals	C57BL/6J mice at 2-10 months old were used. For embryo imaging, BALB/c females and Jcl:ICR females were used.
Wild animals	No wild animals were used in this study.
Reporting on sex	Sex-based analysis was not conducted in this study, because the biodistribution of substrates and luciferase expression levels were assumed to be similar in both sexes.
Field-collected samples	No field-collected samples were used in this study.
Ethics oversight	All experimental protocols and husbandry for mice were approved by the Institutional Animal Care and Use Committee of RIKEN Tsukuba Branch and University of Tsukuba, and all mice were cared for and treated humanely in accordance with the Committee's guiding principles.

Note that full information on the approval of the study protocol must also be provided in the manuscript.